PAPER • OPEN ACCESS

Observation of nonlinear spin dynamics and squeezing in a BEC using dynamic decoupling

New Journal of Physics
The open access journal at the forefront of physics

Deutsche Physikalische Gesellschaft DPG
IOP Institute of Physics

Published in partnership with: Deutsche Physikalische Gesellschaft and the Institute of Physics

OPEN ACCESS

RECEIVED
16 December 2020

REVISED
21 March 2021

ACCEPTED FOR PUBLICATION
12 April 2021

PUBLISHED
7 May 2021

PAPER

Observation of nonlinear spin dynamics and squeezing in a BEC using dynamic decoupling

Hagai Edri[1,*], **Boaz Raz**, **Gavriel Fleurov**, **Roee Ozeri and Nir Davidson**

Department of Physics of Complex Systems, Weizmann Institute of Science, Rehovot 7610001, Israel

[1] Present address: Institut für Quantenoptik und Quanteninformation, Österreichische Akademie der Wissenschaften, Innsbruck, Austria.

[*] Author to whom any correspondence should be addressed.

E-mail: hagai.edri@uibk.ac.at

Keywords: Bose–Einstein condensate, dynamic decoupling, ultracold interactions, spin squeezing

Supplementary material for this article is available online

Abstract

We study the evolution of a Bose–Einstein condensate in a two-state superposition due to inter-state interactions. Using a population imbalanced dynamic decoupling scheme, we measure inter-state interactions while canceling intra-state density shifts and external noise sources. Our measurements show low statistical uncertainties for both magnetic sensitive and insensitive superpositions, indicating that we successfully decoupled our system from strong magnetic noises. We experimentally show that the Bloch sphere representing general superposition states is 'twisted' by inter-state interactions, as predicted in [1, 2] and the twist rate depends on the difference between inter-state and intra-state scattering lengths $a_{22} + a_{11} - 2a_{12}$. We use the non-linear spin dynamics to demonstrate squeezing of Gaussian noise, showing 2.79 ± 0.43 dB squeezing when starting with a noisy state and applying 160 echo pulses, which can be used to increase sensitivity when there are errors in state preparation. Our results allow for a better understanding of inter-atomic potentials in ^{87}Rb. Our scheme can be used for spin-squeezing beyond the standard quantum limit and observing polaron physics close to Feshbach resonances, where interactions diverge, and strong magnetic noises are ever present.

The state of a two-level system can be represented by a vector on the Bloch sphere. Linear operations on this state can be represented by rotations and contractions of the sphere, generated by unitary and non-unitary operations respectively. In cases where the Bloch sphere represents the average state of an ensemble of two-level systems, interactions can introduce non-linear evolution, represented by torsion and one-axis-twist of the sphere. Non-linear spin dynamics can be used for spin-squeezing and generation of non-classical states [1].

In the cold collision regime, interactions are parameterized by s-wave scattering length a_{ij}, where $|i\rangle$, $|j\rangle$ are two internal states of the interacting atoms (i.e. Zeeman states or hyperfine levels). Our knowledge of scattering lengths comes from spectroscopic measurements [2, 3], observations of collective oscillations [4], position of Feshbach resonances [5–7] and thermalization experiments [8, 9], which are used for calibrations of detailed calculations of inter-atomic potentials [10, 11]. Precise knowledge of inter-state interaction parameters, as well as differences in scattering lengths between different i nternal states, is important for spin-squeezing [12, 13], polaron physics [14–17], Bose–Einstein condensate (BEC) solitons [18, 19], and magnetic dipole–dipole interactions [20].

Frequency shifts in population-balanced Ramsey spectroscopy due to mean-field interactions were used to measure intra-state scattering length differences $a_{22} - a_{11}$ for both thermal ultracold bosons [21] and BEC [2] (their absence was observed for both thermal [22] and quantum degenerate [23] ultracold Fermi gases). In population-imbalanced spectroscopy additional frequency shift proportional to $a_{22} + a_{11} - 2a_{12}$

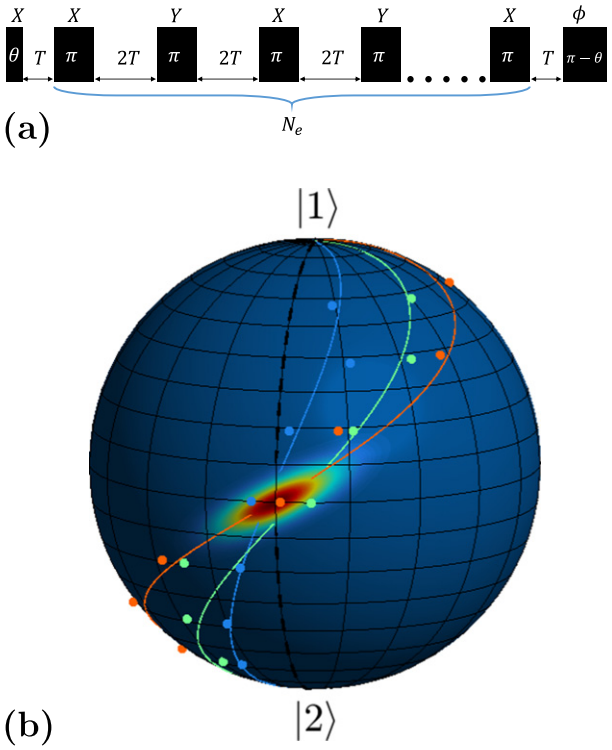

Figure 1. Imbalanced DD. (a) Pulse sequence. An initial pulse of area θ, followed by N_e echo pulses around X, Y axes, separated by time $2T$, and a final pulse with area $\pi - \theta$ and phase ϕ. Initial pulse creates a superposition $\cos\frac{\theta}{2}|1\rangle + \sin\frac{\theta}{2}|2\rangle$, with density difference $\delta n = n\cos\theta$, where n is the total density. (b) A twisted Bloch sphere after imbalanced DD. Measured phase shifts (circles) on magnetic sensitive transition $|1,1\rangle \leftrightarrow |2,0\rangle$ (similar to figure 4) at several latitudes for increasing total evolution times (blue-12.1 ms, green-26.2 ms, orange-54.6 ms). Solid lines are fits to the data. Locally, a coherent state around the equator is squeezed by one-axis-twist, illustrated by the colored distribution.

and to density differences between states was predicted, but was too small to be measured [2]. These measurements were limited to magnetic insensitive transitions, where magnetic noises are largely suppressed. Dynamic decoupling (DD) [24] could decouple the system from these magnetic noises and preserve its coherence over long times by applying a set of spin rotations. It also decouples it from intra-state interactions and can not be applied to measure them.

DD was demonstrated in NMR [25, 26], spins in solids [27–29], ultracold atoms [30, 31], and trapped ions [32–34]. DD aims to decouple a system from its environment. To measure a signal, one needs to modulate the system itself synchronously with the DD scheme [35–37], in a similar fashion to how a lock-in amplifier operates. However, this modulation can generate noises that are in phase with the DD scheme, and requires control of the signal of interest.

In this letter, we propose and demonstrate a method for measuring interactions in ultracold gases in a noisy environment with a long coherence time and increased sensitivity to inter-state interactions. Our measurements are based on a population imbalanced DD scheme (figure 1) that accumulates effects of inter-state interactions between ultracold atoms in two internal states, without adding any modulation besides the DD itself. We fully characterize the process [30], confirming the prediction of [2] that the Bloch sphere is twisted by inter-state interaction. We determine $a_{22} + a_{11} - 2a_{12}$ with $0.02a_0$ uncertainty for both magnetic sensitive and insensitive transitions. Around the equator, this twist generates spin-squeezing. We measured evolution of a state with Gaussian noise around the X axis during DD, showing noise squeezing of 2.79 ± 0.43 dB with weak non-linear interaction. This is relevant when there are initialization errors, and can be used to increase sensitivity.

Our method can also be used for spin-squeezing beyond the standard quantum limit, similar to [12, 13]. Long coherence time achievable in our scheme enables us to generate a spin-squeezed state even with weak interactions. It is also relevant for polaron physics [14–17, 38] and measurements of weak magnetic dipole–dipole interaction [20]. Imbalanced DD can increase coherence in these measurements, which will, in turn, increase spectroscopic resolution.

We use a BEC of ultracold ^{87}Rb atoms in states $|1\rangle = |F = 1, m_{f_1}\rangle$ and $|2\rangle = |F = 2, m_{f_2}\rangle$, where F is the total spin and $m_{f_{1,2}}$ is spin projection along the magnetic field axis. The mean-field energy shifts are:

$$\begin{aligned}\delta E_1 &= \frac{4\pi\hbar^2}{m}(\alpha_{11}a_{11}n_1 + \alpha_{12}a_{12}n_2),\\ \delta E_2 &= \frac{4\pi\hbar^2}{m}(\alpha_{22}a_{22}n_2 + \alpha_{12}a_{12}n_1),\end{aligned} \tag{1}$$

$n_{1,2}$ are densities in different states, a_{ij} are s-wave scattering lengths, α_{ij} are correlation factors accounting for Bose statistics (for thermal clouds $\alpha_{ij} = 2$, and for BEC $\alpha_{ij} = 1$ [2]), m is atomic mass, and $\hbar$ is the reduced Planck constant. The energy difference in a BEC is,

$$\delta E_2 - \delta E_1 = \frac{2\pi\hbar^2}{m}\left((a_{22} - a_{11})(n_1 + n_2) + (2a_{12} - a_{22} - a_{11})(n_1 - n_2)\right). \tag{2}$$

Here, the first term is proportional to the total density $n = n_1 + n_2$, while the second is proportional to the density difference $\delta n = n_1 - n_2$.

In a typical Ramsey experiment atoms are in an equal superposition $\frac{1}{\sqrt{2}}\left(|1\rangle + |2\rangle\right)$ during the interrogation time. Therefore, the second term in equation (2) is eliminated, leaving only contribution proportional to n in the phase shift. We can prepare a density difference by applying a pulse with area $\theta \neq \pi/2$, generating the state $\cos\frac{\theta}{2}|1\rangle + \sin\frac{\theta}{2}|2\rangle$. Here the density difference is $\delta n = n\cos\theta$. Following a hold time T a second pulse with area $\pi - \theta$ converts phase difference $(\delta E_2 - \delta E_1)\,T/\hbar$ into population difference.

In our imbalanced DD scheme (figure 1(a)) we apply a number of echo pulses N_e between two pulses of θ and $\pi - \theta$. Our pulses have a Rabi frequency Ω_R and alternating phases of $0°, 90°$, rotating the state around the Bloch sphere's X, Y axes sequentially. This scheme has several benefits. First, it cancels the first term in equation (2), because n does not change following a π pulse. Second, quasi-static external noises and inhomogeneous dephasing mechanisms (e.g. due to inhomogeneous density or light shift) as well as spatial phase evolution [39] are nullified, allowing for longer coherence time. The echo pulses reverse the sign of δn. Therefore, we accumulate phase due to the second term in equation (2) and achieve an increased sensitivity to $a_{11} + a_{22} - 2a_{12}$, which is typically smaller than $a_{22} - a_{11}$.

The calculated population $P = \frac{N_1}{N_1+N2}$ in state $|2\rangle$ at the end of this sequence, is given by [40]

$$P = \frac{1}{4}\left[2\sin^2\theta\,\cos\left(\phi + \frac{gn}{\hbar}N_eT\,\cos\theta\right) + \cos 2\theta + 3\right], \tag{3}$$

where ϕ is the last pulse phase and $g = \frac{4\pi\hbar^2}{m}(a_{11} + a_{22} - 2a_{12})$ is the interaction shift. The calculation does not take into account any decoherence or atom loss during the process. The interaction twists the Bloch sphere (figure 1(b)), where the upper hemisphere ($\theta < \pi/2$) and lower hemisphere ($\theta > \pi/2$) rotate in opposite directions. Measured phase shifts (circles) at different latitudes show progress for increasing evolution times (blue-12.1 ms, green-26.2 ms, orange-54.6 ms).

Interactions are negligible compared to the Rabi frequency ($\frac{gn}{\hbar} \ll \Omega_R$, [40]) and are neglected during the echo pulses. Rotating the Bloch vector around X, Y cancels noises in control pulses [28, 41, 42] and also renders the rotations symmetric with respect to the Bloch sphere equator in every $XYXY$ block. Any residual phase accumulated due to population imbalance during the pulses is equal in the upper and lower Bloch hemispheres.

In our system we trap a BEC of $\sim 5\times10^5$ ^{87}Rb atoms in a crossed dipole trap with trapping frequencies of $(\omega_x, \omega_y, \omega_z) = 2\pi \times (31, 37, 109)$ Hz. We use MW radiation close to 6.834 GHz to drive transitions between hyperfine levels in a magnetic field of 2.07 G. We drive both magnetic insensitive transition $|1,0\rangle \leftrightarrow |2,0\rangle$ and magnetic sensitive transitions $|1,1\rangle \leftrightarrow |2,0\rangle$, $|1,1\rangle \leftrightarrow |2,2\rangle$, which are separated by a large Zeeman splitting $\Delta \gg \Omega_R$.

To perform an imbalanced DD scheme, we start with all atoms in state $|1\rangle = |1,0\rangle$ (magnetic insensitive transition) or $|1\rangle = |1,1\rangle$ (magnetic sensitive transitions) and apply MW pulses to couple to state $|2\rangle = |2,0\rangle$ or $|2\rangle = |2,2\rangle$. We apply a pulse of length t_p to rotate the Bloch vector around the X axis with a polar angle $\theta = \Omega_R t_p$. After hold time T we apply a π pulse to invert populations. We then alternate between π pulses around the X and Y axes with hold time of $2T$ in between ($XY8$ sequence [43]). Finally, after another hold time T we apply a $\pi - \theta$ pulse with phase ϕ, rotating the vector around the axis $\cos\phi\cdot\hat{x} - \sin\phi\cdot\hat{y}$. An illustration of our pulse sequence is shown in figure 1(a). The train of echo pulses can be prolonged to accumulate more phase and increase sensitivity to g. We used up to 72 echo pulses.

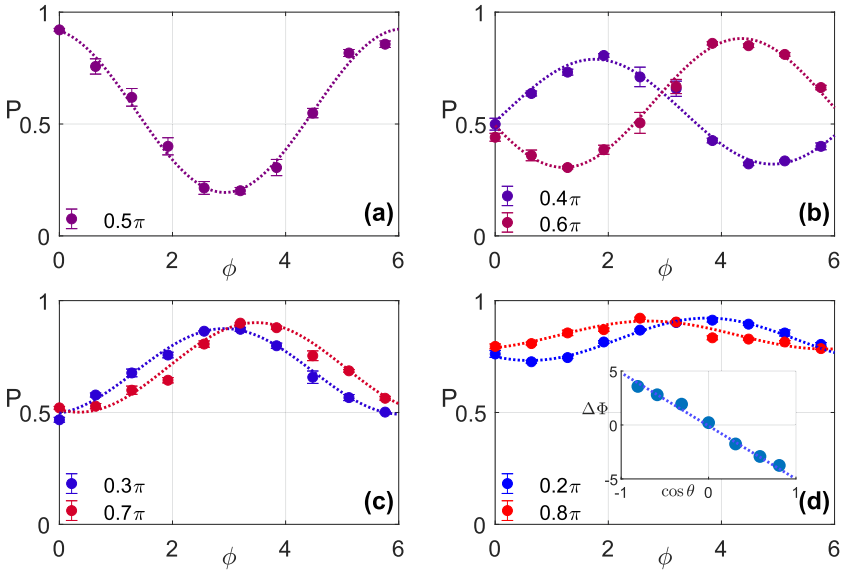

Figure 2. Imbalanced DD on $|1,0\rangle \leftrightarrow |2,0\rangle$ transition, with 16 echo pulses and hold time $T = 2.88$ ms, giving a total time of 92 ms. (a)–(d) Measured population P (circles) while scanning ϕ for different θ, showing clear fringes and high contrast. The fringes are phase shifted due to inter-state interactions and density difference $\delta n/n = \cos\theta$. Dotted lines are fits to the data, error bars indicate one standard deviation from four repeated measurements. ((d), inset) Phase shift extracted from (a)–(d) fits (circles) is proportional to $\cos\theta$ as predicted by equation (3), dotted line is a linear fit.

After the final pulse we release the cloud from the trap and let it expand for 20 ms. We measure population in state $|2\rangle$ using a normalized detection scheme [40]. We measure the cloud size and extract chemical potential and average density.

Our measurements on magnetic insensitive transition ($|1,0\rangle \leftrightarrow |2,0\rangle$) after 16 echo pulses with hold time $T = 2.88$ ms (total time of 92 ms) are shown in figures 2(a)–(d), filled circles are measured populations vs ϕ, where different colors indicate different polar angles θ. To take into account decoherence that depend on the population in $F = 2$ manifold [40], which is not accounted for in equation (3). We fit data points with a constant θ to the function $C\cos(\phi + \Delta\Phi) + B$ (dotted lines), where ϕ is the final pulse phase, $\Delta\Phi$ is the phase shift, C is the contrast and B is the bias. The high contrast of figure 2(a) ($\theta = \pi/2$) indicates high coherence after a long DD time of 92 ms, compared with our typical Ramsey coherence time (i.e. contrast decay to $1/e$) of ∼20 ms. The contrast decreases with θ, as expected from equation (3), but the fringes are clear (figures 2(b)–(d)) with excellent agreement with our fits. All measurements shows a phase shift proportional to $\cos\theta$ (figure 2(d), inset) as predicted by equation (3).

To validate our measurement and test the performance of this sequence, we repeated this measurement for different times $T_{\rm tot} = 2N_{\rm e}T$, varying T and $N_{\rm e}$. Our measurement time was limited by inelastic collisions of atoms in state $|2,0\rangle$, transferring them to states $|2,-1\rangle$ and $|2,1\rangle$ [44]. The frequency shift we measured $\frac{\Delta\Phi}{2\pi N_{\rm e}T}$ grows linearly with δn (figure 3). From a linear fit we extract $(a_{11}+a_{22}-2a_{12})_{1,0\to2,0} = -1.17 \pm 0.02a_0$ (statistical error of one standard deviation), showing the high precision and SNR achieved with imbalanced DD. Our main source of systematic errors is density uncertainty, which we estimate to be 16% [40, 45]. Using Ramsey spectroscopy we measured $(a_{22} - a_{11})_{1,0\to2,0} = -3.4 \pm 0.2a_0$, combining the two measurements we get $\left(\frac{a_{11}+a_{22}-2a_{12}}{a_{22}-a_{11}}\right)_{1,0\to2,0} = 0.34 \pm 0.02$ which is insensitive to density, and comparable with another recent measurement [20]. This measurement of scattering length difference is useful for calculating interatomic potentials.

To show the ability of DD in a noisy environment, we performed the same measurements on magnetic sensitive transitions, $|1,1\rangle \leftrightarrow |2,0\rangle$ and $|1,1\rangle \leftrightarrow |2,2\rangle$ with magnetic field sensitivity of 0.7 kHz mG^{-1} and 2.1 kHz mG^{-1} respectively. Our main magnetic noise source was the 50 Hz AC from the electrical grid of 1.31 ± 0.12 mG peak to peak at the atoms position [40], which is comparable to our Rabi frequency of ∼7 kHz for these transitions. Our results for the $|1,1\rangle \leftrightarrow |2,0\rangle$ transition with 56 echo pulses and $T = 0.38$ ms (figure 4), are similar to our results for magnetic insensitive transition. Even in the presence of strong noises our results show long coherence times and phase shifts linear with δn (figure 4(d), inset). Our Ramsey coherence time for magnetic sensitive transition is limited to ∼1 ms. With DD we were able to measure fringes with high contrast after a total time of 54.6 ms for $|1,1\rangle \leftrightarrow |2,0\rangle$ transition and 45.9 ms for $|1,1\rangle \leftrightarrow |2,2\rangle$ transition.

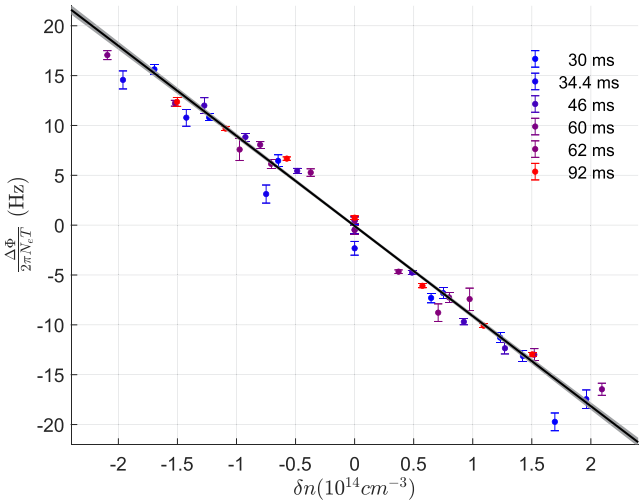

Figure 3. Frequency shift due to interactions between $|1,0\rangle \leftrightarrow |2,0\rangle$—measured frequency shift $\frac{\Delta\Phi}{2\pi N_e T}$ and density difference δn from measurements of imbalanced DD with various total evolution times $T_{\rm tot} = 2N_e T$ (indicated in figure legend). A linear fit (black line, one standard deviation in gray) yields scattering length difference of $(a_{11} + a_{22} - 2a_{12})_{1,0\to 2,0} = -1.17 \pm 0.02 a_0$, showing the high precision achieved with this method.

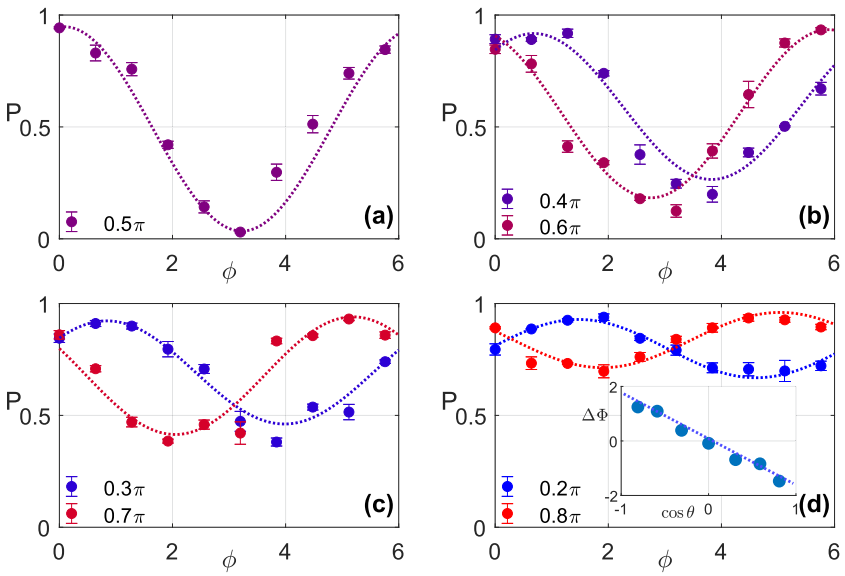

Figure 4. Imbalanced DD on magnetic sensitive transition $|1,1\rangle \leftrightarrow |2,0\rangle$, with 56 echo pulses and hold time $T = 0.38$ ms, giving a total time of 42.4 ms. Short hold time T is needed to decouple from strong magnetic noises. (a)–(d) Measured population P while scanning ϕ for different θ. Showing fringes with high coherence, even in the presence of strong magnetic noises. ((d), inset) Phase shift taken form (a)–(d) fits (circles), showing a linear dependence (dotted line) on population imbalance $\cos\theta$, similar to the magnetic insensitive measurements (figure 2).

We repeated this measurement for different times $T_{\rm tot}$, varying T and N_e for the magnetic sensitive transitions, and measured a frequency shift that grows linearly with the density difference (figure 5). From a linear fit we extract $(a_{11} + a_{22} - 2a_{21}) = -0.76 \pm 0.02 a_0$ for $|1,1\rangle \to |2,0\rangle$ (figure 5(a)) transition and $(a_{11} + a_{22} - 2a_{21}) = 0.22 \pm 0.04 a_0$ for $|1,1\rangle \to |2,2\rangle$ transition (figure 5(b)), demonstrating high precision and SNR even in a noisy environment.

When comparing the measurements for all three transitions with calculated scattering lengths [46], our results are within a factor of 2 from the theory for $|1,0\rangle \to |2,0\rangle$ and $|1,1\rangle \to |2,0\rangle$ transitions, and within a factor of 5 for the $|1,1\rangle \to |2,2\rangle$ transition. Our method is applicable close to a Feshbach resonance where typically there are no magnetic insensitive transitions and one of the scattering lengths diverges. This will result in larger phase shifts and can be used to generate spin-squeezed states [12, 13].

To show a potential application of our scheme for spin-squeezing we demonstrate squeezing of a state with Gaussian noise, which emulates initialization errors. Here we used the magnetic insensitive transition $|1,0\rangle \leftrightarrow |2,0\rangle$. We prepared a state with a symmetric Gaussian noise around the X axis of the Bloch sphere

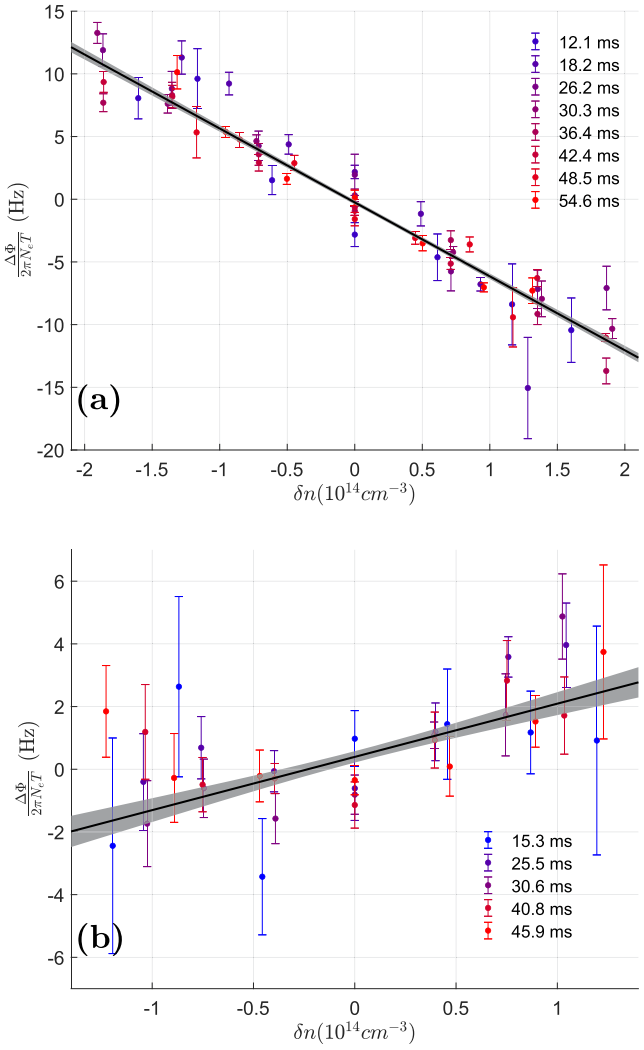

Figure 5. Frequency shift due to interactions in magnetic sensitive transitions—the measured frequency shift $\frac{\Delta\Phi}{2\pi N_e T}$ and density difference δn from imbalanced DD with various N_e and T, for $|1,1\rangle \leftrightarrow |2,0\rangle$ (a) and $|1,1\rangle \leftrightarrow |2,2\rangle$ (b)transitions. A linear fit (black line, one standard deviation in gray) gives a scattering length difference of (a) $(a_{11}+a_{22}-2a_{12})_{1,1\to2,0} = -0.76 \pm 0.02 a_0$ and (b) $(a_{11}+a_{22}-2a_{12})_{1,1\to2,2} = 0.22 \pm 0.04 a_0$ showing the high precision achieved in this method even in the presence of strong magnetic noise.

by starting in state $|1,0\rangle$ and applying a pulse of $\frac{\pi}{2}(1+\varepsilon_\theta)$ with a phase $\frac{\pi}{2}(1+\varepsilon_\phi)$, where $\varepsilon_\phi, \varepsilon_\theta$ are randomly chosen errors (< 1) from a Gaussian distribution, in pulse length and phase, respectively. We carried out a DD scheme of concatenated $XY8$ blocks with hold time of $2T$ between echo pulses. After this pulse sequence, the state remains centered on the X axis. We then applied a final pulse to rotate the state around the X axis with angle β and measured population. We repeated this sequence with different T to see how the twisting dynamics changes the statistical variance in population σ_p^2 as we scan β.

In figure 6 we show our results for added Gaussian noise of 25% in state preparation and $N_e = 160$. For short times ($T = 2.5\ \mu$s, $T_{tot} = 0.8$ ms, red) the variance does not change significantly with β. For long times ($T = 200\ \mu$s, $T_{tot} = 64$ ms, blue) we see a double peak feature, with a decrease in variance at angle $\beta_\circ = 218 \pm 14°$. From a fit to the data we extract 2.79 ± 0.43 dB noise squeezing at $\beta_\circ$, comparing short and long times. After decreasing detection noise we have 3.02 ± 0.47 dB noise squeezing (to quantify the detection noise, we measured the population after one $\pi/2$ pulse for different β). This measurement demonstrates our ability to squeeze symmetric Gaussian noise in a specific direction using DD with a weak nonlinear interaction. This method can increase sensitivity in the presence of initialization errors and for spin-squeezing beyond the standard quantum limit.

In conclusion, we introduced and demonstrated imbalanced DD as a robust method with high contrast and long coherence time. For magnetic insensitive transition, where dephasing is mainly due to interactions in the inhomogenous cloud, we increase the coherence time by a factor of $\sim$10. While for magnetic sensitive transition, where strong magnetic noise at 50 Hz is the main cause for dephasing, we increase the coherence time by a factor of $\sim$50. To scale up and further increase the coherence time, we need to increase the

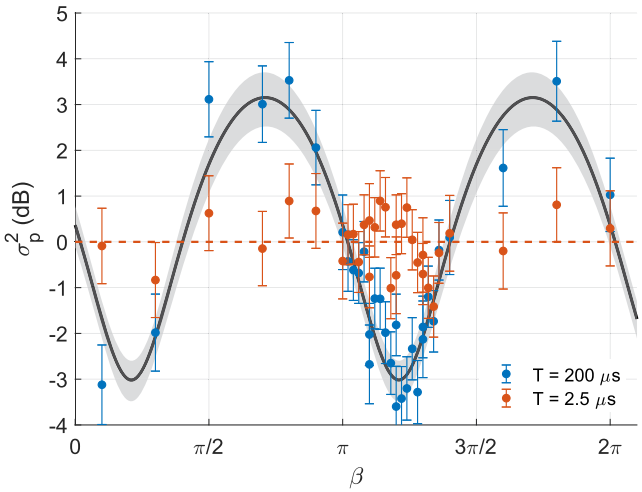

Figure 6. Gaussian noise squeezing. Population variance σ_p^2 when rotating a state around the X axis with angle β after DD with 160 echo pulses. For short hold time ($T = 2.5$ μs, red) we get a constant variance, which is used for scaling the vertical axis. For long hold time ($T = 200$ μs, blue), we see a double peak feature, using a fit to our data [1] (black line, one standard deviation in gray) we extract maximal squeezing of 2.79 ± 0.43 dB at an angle $\beta_\circ = 218 \pm 14°$, compared to short hold time mean population variance.

number of pulses significantly, which can be challenging as control errors become dominant. Using shortcut to adiabaticity techniques [47], we could apply fast frequency sweeps, which are more robust against these errors.

We implemented imbalanced DD to measure interactions in a BEC and the Bloch sphere twist caused by them. Our precision is comparable to other measurements done on a magnetic insensitive transition $|1,-1\rangle \leftrightarrow |2,1\rangle$ [2, 4], and we show similar precision with magnetic sensitive transitions. The scattering length difference we measured for three transitions in ^{87}Rb is useful for calculating interatomic potentials. The interactions between imbalanced populations generate a phase shift that is accumulated in our sequence without having to externally perturb the system, as in other DD schemes [35, 36]. This type of interactions are of great interest close to Feshbach resonances, where scattering length diverges, and magnetic field noise is dominant. We demonstrated spin-squeezing of a state with Gaussian noise using DD and weak nonlinear interactions, showing reduced uncertainty when rotating our final state in a specific angle. This can be useful for measurements with initialization errors.

Acknowledgments

The authors would like to thank Eite Tiesinga, Yotam Shapira and Tom Manovitz for fruitful discussions. This work was supported by the Israeli Science Foundation, the Israeli Ministry of Science Technology and Space and the Minerva Stiftung.

Data availability statement

The data that support the findings of this study are available upon reasonable request from the authors.

ORCID iDs

Hagai Edri https://orcid.org/0000-0001-5035-4307
Boaz Raz https://orcid.org/0000-0002-7892-6335
Gavriel Fleurov https://orcid.org/0000-0002-1750-6177

References

[1] Kitagawa M and Ueda M 1993 Squeezed spin states *Phys. Rev.* A **47** 5138
[2] Harber D M, Lewandowski H J, McGuirk J M and Cornell E A 2002 Effect of cold collisions on spin coherence and resonance shifts in a magnetically trapped ultracold gas *Phys. Rev.* A **66** 053616

[3] Fertig C and Gibble K 2000 Measurement and cancellation of the cold collision frequency shift in an ^{87}Rb fountain clock *Phys. Rev. Lett.* **85** 1622
[4] Egorov M, Opanchuk B, Drummond P, Hall B V, Hannaford P and Sidorov A I 2013 Measurement of *s*-wave scattering lengths in a two-component Bose–Einstein condensate *Phys. Rev.* A **87** 053614
[5] Knoop S, Schuster T, Scelle R, Trautmann A, Appmeier J, Oberthaler M K, Tiesinga E and Tiemann E 2011 Feshbach spectroscopy and analysis of the interaction potentials of ultracold sodium *Phys. Rev.* A **83** 042704
[6] Ferlaino F, D'Errico C, Roati G, Zaccanti M, Inguscio M, Modugno G and Simoni A 2006 Feshbach spectroscopy of a K-Rb atomic mixture *Phys. Rev.* A **73** 040702
[7] Kerman A J, Chin C, Vuletić V, Chu S, Leo P J, Williams C J and Julienne P S 2001 Determination of Cs–Cs interaction parameters using Feshbach spectroscopy *C. R. Acad. Sci. IV* **2** 633–9
[8] Marzok C, Deh B, Courteille P W and Zimmermann C 2007 Ultracold thermalization of ^{7}Li and ^{87}Rb *Phys. Rev.* A **76** 052704
[9] Ferrari G, Inguscio M, Jastrzebski W, Modugno G, Roati G and Simoni A 2002 Collisional properties of ultracold K-Rb mixtures *Phys. Rev. Lett.* **89** 053202
[10] Van Kempen E G M, Kokkelmans S J J M F, Heinzen D J and Verhaar B J 2002 Interisotope determination of ultracold rubidium interactions from three high-precision experiments *Phys. Rev. Lett.* **88** 093201
[11] Verhaar B J, Van Kempen E G M and Kokkelmans S J J M F 2009 Predicting scattering properties of ultracold atoms: adiabatic accumulated phase method and mass scaling *Phys. Rev.* A **79** 032711
[12] Gross C, Zibold T, Nicklas E, Estève J and Oberthaler M K 2010 Nonlinear atom interferometer surpasses classical precision limit *Nature* **464** 1165
[13] Riedel M F, Böhi P, Li Y, Hänsch T W, Sinatra A and Treutlein P 2010 Atom-chip-based generation of entanglement for quantum metrology *Nature* **464** 1170–3
[14] Kohstall C, Zaccanti M, Jag M, Trenkwalder A, Massignan P, Bruun G M, Schreck F and Grimm R 2012 Metastability and coherence of repulsive polarons in a strongly interacting Fermi mixture *Nature* **485** 615
[15] Schirotzek A, Wu C-H, Sommer A and Zwierlein M W 2009 Observation of Fermi polarons in a tunable Fermi liquid of ultracold atoms *Phys. Rev. Lett.* **102** 230402
[16] Hu M-G, Van de Graaff M J, Kedar D, Corson J P, Cornell E A and Jin D S 2016 Bose polarons in the strongly interacting regime *Phys. Rev. Lett.* **117** 055301
[17] Jørgensen N B, Wacker L, Skalmstang K T, Parish M M, Levinsen J, Christensen R S, M Bruun G and Jan J A 2016 Observation of attractive and repulsive polarons in a Bose–Einstein condensate *Phys. Rev. Lett.* **117** 055302
[18] Hamner C, Zhang Y, Chang J J, Zhang C and Engels P 2013 Phase winding a two-component Bose–Einstein condensate in an elongated trap: experimental observation of moving magnetic orders and dark-bright solitons *Phys. Rev. Lett.* **111** 264101
[19] Bersano T M, Gokhroo V, Khamehchi M A, D'Ambroise J, Frantzeskakis D J, Engels P and Kevrekidis P G 2018 Three-component soliton states in spinor $f = 1$ bose-einstein condensates *Phys. Rev. Lett.* **120** 063202
[20] Zou Y-Q, Bakkali-Hassani B, Maury C, Le Cerf É, Nascimbene S, Dalibard J and Beugnon J 2020 Magnetic dipolar interaction between hyperfine clock states in a planar alkali Bose gas *Phys. Rev. Lett.* **125** 233604
[21] Gibble K and Chu S 1993 Laser-cooled Cs frequency standard and a measurement of the frequency shift due to ultracold collisions *Phys. Rev. Lett.* **70** 1771–4
[22] Zwierlein M W, Hadzibabic Z, Gupta S and Ketterle W 2003 Spectroscopic insensitivity to cold collisions in a two-state mixture of Fermions *Phys. Rev. Lett.* **91** 250404
[23] Gupta S, Hadzibabic Z, Zwierlein M W, Stan C A, Dieckmann K, Schunck C H, Van Kempen E G M, Verhaar B J and Ketterle W 2003 Radio-frequency spectroscopy of ultracold Fermions *Science* **300** 1723–6
[24] Lidar D A 2014 Review of decoherence-free subspaces, noiseless subsystems, and dynamical decoupling *Adv. Chem. Phys.* **154** 295–354
[25] Haar D 1962 *Fluctuation, Relaxation and Resonance in Magnetic Systems: Scottish Universities' Summer School 1961* (Edinburgh: Oliver & Boyd)
[26] Ulrich H 1976 *High Resolution NMR in Solids: Advances in Magnetic Resonance* (New York: Academic)
[27] Du J, Rong X, Zhao N, Wang Y, Yang J and Liu R B 2009 Preserving electron spin coherence in solids by optimal dynamical decoupling *Nature* **461** 1265
[28] De Lange G, Wang Z H, Riste D, Dobrovitski V V and Hanson R 2010 Universal dynamical decoupling of a single solid-state spin from a spin bath *Science* **330** 60–3
[29] Bar-Gill N, Pham L M, Jarmola A, Budker D and Walsworth R L 2013 Solid-state electronic spin coherence time approaching one second *Nat. Commun.* **4** 1743
[30] Sagi Y, Almog I and Davidson N 2010 Process tomography of dynamical decoupling in a dense cold atomic ensemble *Phys. Rev. Lett.* **105** 053201
[31] Almog I, Sagi Y, Gordon G, Bensky G, Kurizki G and Davidson N 2011 Direct measurement of the system-environment coupling as a tool for understanding decoherence and dynamical decoupling *J. Phys. B: At. Mol. Opt. Phys.* **44** 154006
[32] Kotler S, Akerman N, Glickman Y and Ozeri R 2013 Nonlinear single-spin spectrum analyzer *Phys. Rev. Lett.* **110** 110503
[33] Shaniv R, Akerman N and Ozeri R 2016 Atomic quadrupole moment measurement using dynamic decoupling *Phys. Rev. Lett.* **116** 140801
[34] Biercuk M J, Uys H, VanDevender A P, Shiga N, Itano W M and Bollinger J J 2009 Optimized dynamical decoupling in a model quantum memory *Nature* **458** 996
[35] Kotler S, Akerman N, Glickman Y, Keselman A and Ozeri R 2011 Single-ion quantum lock-in amplifier *Nature* **473** 61
[36] Shaniv R and Ozeri R 2017 Quantum lock-in force sensing using optical clock Doppler velocimetry *Nat. Commun.* **8** 14157
[37] de Lange G, Ristè D, Dobrovitski V V and Hanson R 2011 Single-spin magnetometry with multipulse sensing sequences *Phys. Rev. Lett.* **106** 080802
[38] Ness G, Shkedrov C, Florshaim Y, Diessel O K, von Milczewski J, Schmidt R and Sagi Y 2020 Observation of a smooth polaron-molecule transition in a degenerate Fermi gas *Phys. Rev.* X **10** 041019
[39] Anderson R P, Ticknor C, Sidorov A I and Hall B V 2009 Spatially inhomogeneous phase evolution of a two-component Bose–Einstein condensate *Phys. Rev.* A **80** 023603
[40] See supplemental material (https://stacks.iop.org/NJP/23/053005/mmedia)
[41] Gullion T, Baker D B and Conradi M S 1969 New, compensated Carr–Purcell sequences *J. Magn. Reson.* **89** 479–84
[42] Wang Z-H, De Lange G, Ristè D, Hanson R and Dobrovitski V V 2012 Comparison of dynamical decoupling protocols for a nitrogen-vacancy center in diamond *Phys. Rev.* B **85** 155204

[43] Mustafa A A, Álvarez G A and Suter D 2013 Robustness of dynamical decoupling sequences *Phys. Rev.* A **87** 042309
[44] Widera A, Gerbier F, Fölling S, Gericke T, Mandel O and Bloch I 2006 Precision measurement of spin-dependent interaction strengths for spin-1 and spin-2 ^{87}Rb atoms *New J. Phys.* **8** 152
[45] Edri H, Raz B, Matzliah N, Davidson N and Ozeri R 2020 Observation of spin–spin Fermion-mediated interactions between ultracold bosons *Phys. Rev. Lett.* **124** 163401
[46] Tiesniga E 2020 private communication
[47] Guéry-Odelin D, Ruschhaupt A, Kiely A, Torrontegui E, Martínez-Garaot S and Muga J G 2019 Shortcuts to adiabaticity: concepts, methods, and applications *Rev. Mod. Phys.* **91** 045001